

LETTER • **OPEN ACCESS**

Global assessment of spatiotemporal changes of frequency of terrestrial wind speed

To cite this article: Yanan Zhao *et al* 2023 *Environ. Res. Lett.* **18** 044048

View the [article online](#) for updates and enhancements.

You may also like

- [An initial study of complete 2D shear wave dispersion images using a reverberant shear wave field](#)
Juvenal Ormachea, Kevin J Parker and Richard G Barr
- [A fast and quantitative measurement of shear wave speed and attenuation using \(cross\) modal assurance criterion for acoustic radiation force elasticity imaging](#)
Yang Jiao, Chen Yang, Jie Xu et al.
- [An analysis of intrinsic variations of low-frequency shear wave speed in a stochastic tissue model: the first application for staging liver fibrosis](#)
Yu Wang, Min Wang and Jingfeng Jiang



The Breath Biopsy® Guide
Fourth edition

FREE

DOWNLOAD THE FREE E-BOOK

BREATH BIOPSY

OWLSTONE MEDICAL

ENVIRONMENTAL RESEARCH
LETTERS

LETTER

Global assessment of spatiotemporal changes of frequency
of terrestrial wind speed

OPEN ACCESS

RECEIVED
18 January 2023REVISED
15 March 2023ACCEPTED FOR PUBLICATION
3 April 2023PUBLISHED
17 April 2023

Original content from
this work may be used
under the terms of the
[Creative Commons
Attribution 4.0 licence](#).

Any further distribution
of this work must
maintain attribution to
the author(s) and the title
of the work, journal
citation and DOI.

Yanan Zhao¹ , Shijing Liang¹ , Yi Liu¹ , Tim R McVicar² , Cesar Azorin-Molina³ , Lihong Zhou¹,
Robert J H Dunn⁴ , Sonia Jerez⁵ , Yingzuo Qin¹, Xinrong Yang¹ , Jiayu Xu¹ and Zhenzhong Zeng^{1,*}¹ School of Environmental Science and Engineering, Southern University of Science and Technology, Shenzhen, People's Republic of China² CSIRO Environment, Black Mountain, Canberra, ACT, Australia³ Centro de Investigaciones sobre Desertificación—Spanish National Research Council (CIDE, CSIC-UV-Generalitat Valenciana), Moncada, Valencia, Spain⁴ Centro de Investigaciones sobre Desertificación, Consejo Superior de Investigaciones Científicas (CIDE, CSIC-UV-Generalitat Valenciana), Climate, Atmosphere and Ocean Laboratory (Climatoc-Lab), Moncada, Valencia, Spain⁵ Department of Physics, University of Murcia, Murcia, Spain

* Author to whom any correspondence should be addressed.

E-mail: zengzz@sustech.edu.cn**Keywords:** wind speed, frequency changes, wind energy, power curve, strong windsSupplementary material for this article is available [online](#)**Abstract**

Wind energy, an important component of clean energy, is highly dictated by the disposable wind speed within the working regime of wind turbines (typically between 3 and 25 m s⁻¹ at the hub height). Following a continuous reduction ('stilling') of global annual mean surface wind speed (SWS) since the 1960s, recently, researchers have reported a 'reversal' since 2011. However, little attention has been paid to the evolution of the effective wind speed for wind turbines. Since wind speed at hub height increases with SWS through power law, we focus on the wind speed frequency variations at various ranges of SWS through hourly *in-situ* observations and quantify their contributions to the average SWS changes over 1981–2021. We found that during the stilling period (here 1981–2010), the strong SWS (≥ 5.0 m s⁻¹, the 80th of global SWS) with decreasing frequency contributed 220.37% to the continuous weakening of mean SWS. During the reversal period of SWS (here 2011–2021), slight wind (0 m s⁻¹ < SWS < 2.9 m s⁻¹) contributed 64.07% to a strengthening of SWS. The strengthened strong wind (≥ 5.0 m s⁻¹) contributed 73.38% to the trend change of SWS from decrease to increase in 2010. Based on the synthetic capacity factor series calculated by considering commercial wind turbines (General Electric GE 2.5-120 model with rated power 2.5 MW) at the locations of the meteorological stations, the frequency changes resulted in a reduction of wind power energy (-10.02 TWh yr⁻¹, $p < 0.001$) from 1981 to 2010 and relatively weak recovery (2.67 TWh yr⁻¹, $p < 0.05$) during 2011–2021.

1. Introduction

Wind energy is a key component of the energy market and a potential way for climate mitigation (IEA 2020). In 2021, the global wind industry reached 94 GW power capacity addition, mainly driven by China, Europe and the United States (Global Wind Energy Council 2022). Yet, the current installation rates suggest that it will still be challenging to meet the 1.5 °C mitigation goal (Global Wind Energy Council 2022). To promote wind energy expansion, understanding the efficiency of wind power generation is necessary.

Wind power generation is particularly sensitive to changes in wind speed as wind power is proportional to the cubic of wind speed (McElroy *et al* 2009, Sohoni *et al* 2016, Eureka *et al* 2017, Pryor *et al* 2020). Global annual mean near-surface wind speed (SWS) continuously declined over the past five decades before 2010, known as the period of 'stilling' (Roderick *et al* 2007, Vautard *et al* 2010, McVicar *et al* 2012), with a decrease rate of -0.08 m s⁻¹ decade⁻¹ during 1978–2010 (Zeng *et al* 2019). But during the past ten years (i.e. 2011 to ~2021), such stilling phenomenon has been replaced by a 'reversal', with an increasing

annual mean SWS of $0.24 \text{ m s}^{-1} \text{ decade}^{-1}$ since (Zeng *et al* 2019). However, how these SWS changes govern wind power generation is uncertain.

Average SWS changes can be insufficient for accurately assessing the wind power generation change relating to the stilling and reversal periods, given that wind power generation on a global scale depends on the effective SWS characterized by its range, frequency, and distribution. Generally, wind speed ranging from 3 to 25 m s^{-1} at the hub height is effective in wind power generation. Specifically, light winds may fail to rotate the turbine blades, while strong winds force wind turbines to shut down to prevent damage (Lydia *et al* 2014). Moreover, most wind power is produced by the SWS within the upper half of the wind speed frequency distribution (Pryor and Barthelmie 2010), which is typically positively skewed (Jung and Schindler *et al* 2019a). To quantify the portion of effective SWS evolution affecting generating wind power generation, wind frequency must be considered. However, previous studies assessing wind frequency change often ignored the statistical distribution of SWS (e.g. Vautard *et al* 2010, Zha *et al* 2017), leading to unrealistic assessments of its influence on wind power generation.

To fill these gaps, here we use the hourly SWS data from Hadley Centre Integrated Surface Database (HadISD, Dunn *et al* 2014, 2016) to derive global and continental wind speed trends, to perform a comprehensive analysis of SWS frequency change over 1981 to 2021. SWS was divided into nine ranges (see details in section 2.2) to analyze the year-to-year SWS frequency variations and quantify the influence of frequency variations on the annual average SWS. We also used the power law to extrapolate the SWS to the wind speed at the hub height of a commercial wind turbine to perform a power assessment and evaluate the effect of SWS frequency changes on wind power generation. Our research proposes a new method to quantify the influence of frequency changes in average SWS changes. We revealed that the weakening of strong wind was the main cause of global 'stilling' and the slight winds are major parts of the SWS reversal.

2. Data and methods

2.1. Dataset

We use the hourly SWS data provided by HadISD (Dunn *et al* 2014, 2016), which is a subset of the station data from the Integrated Surface Database (ISD, Smith *et al* 2011). These data were subject to a series of quality control procedures, including duplicate checks, neighbor outliers and distribution gap checks, to eliminate bad data and maintain data continuity (Dunn *et al* 2016). The HadISD has been used for the annual monitoring of wind in the Bulletin of the America Meteorological Society State in recent years (Dunn *et al* 2016) and has been widely used in previous studies (Woolway *et al* 2019, Zhou

et al 2021, Millstein *et al* 2022). It is noteworthy that Dunn *et al* (2022a) reported on erroneously missing calm winds ($\text{SWS} = 0 \text{ m s}^{-1}$) in the ISD and hence the HadISD since May 2013 for many stations outside of North America, which has an impact on the magnitude of the reversal in winds occurring approximately at the same time (see text S1 and figure S1 in the supplementary information for more detail, Dunn *et al* 2022a). A simple correction was applied for the HadISD in version v3.3.0.202201p and later, which recovers many of the missing observations, and our analyses are based on this corrected version (v3.3.0.202202p).

2.2. Methods

2.2.1. Homogenization and resample of SWS data

To ensure the continuity of the long-term decadal analysis of SWS frequency, we implemented strict selection criteria for SWS time series to use a final subset of qualified stations. The final subset of stations is required to meet the following standards: (1) each final station needs to have continuous monthly records over 1981–2021; (2) each month should have more than 15 d of records; (3) the daily values must have at least four observations. After the data selection, the final subset of stations includes 1511 stations in version (v3.3.0.202202p, see figure S1(c) for station locations).

To obtain the frequency of SWS, we resampled the time series data to address the issue that the observations have inconstant observation intervals. According to appendix figures S2 and S3, the observation intervals vary from 8 h to 1 h for most stations, and some stations have shorter observation intervals since 1990; the standard deviation of the observation intervals is greater than 0.8 h for about 40% of the stations, implying variable observation intervals in one year. Uneven observation intervals introduce biases when counting frequencies of SWS on the annual scale. Therefore, it becomes necessary to transform SWS into equally time-spaced data. Here, we fill the time gap by repeating the later value in the time gap. The biases caused by this resampling method will be discussed in supplementary text S2 and figures S4 and 5.

2.2.2. Wind speed classification criteria

Cut-in and cut-out wind speeds are considered to decide the classification criteria for categorizing the SWS in power generation. The cut-in wind speed, denoted as v_i' , refers to the minimum wind speed that results in the turbine to commencing rotating and generating electricity. The cut-out wind speed, marked as v_f' , is the maximum wind speed to generate usable power. The cut-in and cut-out wind speeds refer to the wind speed at the hub height of the wind turbine. Here we use the parameters of the General Electric GE 2.5-120 wind turbine model (2.5 MW, 120 m diameter, hub height at

Table 1. The classification criteria of SWS. The cut-in wind speed transformed from hub height (110 m) to ground (10 m) is 2.2 m s^{-1} and the cut-in wind speed transformed from hub height (110 m) to ground (10 m) is 17.7 m s^{-1} . Here, square brackets denote closed intervals, and round brackets denote open intervals. For example, the wind speed in class 3 is $2.2 \text{ m s}^{-1} \leq \text{SWS} < 2.9 \text{ m s}^{-1}$.

| Class | 1 | 2 | 3 | 4 | 5 | 6 | 7 | 8 | 9 |
|----------------------------------|---|---------|-----------|-----------|-----------|-----------|-----------|------------|-------|
| Wind speed (m s^{-1}) | 0 | (0–2.2) | [2.2–2.9) | [2.9–3.5) | [3.5–4.1) | [4.1–5.0) | [5.0–6.2) | [6.2–17.7) | >17.7 |

110 m and 139 m) with v_i' of 3.0 m s^{-1} and v_f' of 25.0 m s^{-1} (<https://en.wind-turbine-models.com/turbines/310-ge-general-electric-ge-2.5-120>).

The exponential wind profile power-law relation is applied to transform v_i' and v_f' at 110 m height from the 10 m wind speed records. The power-law relationship can be expressed as follows:

$$u_{tb} = u_s \left(\frac{z_{tb}}{z_s} \right)^\alpha \tag{1}$$

where u_{tb} and u_s represent wind speed at height z_{tb} (110 m) and z_s (10 m), and α is a nondimensional parameter usually assumed to be constant 1/7, which is broadly applicable to low surface roughness and adopted by some studies involving wind power assessment (Islam et al 2011, Wang et al 2016, Liu et al 2019). The cut-in (v_i) and cut-out (v_f) wind speeds at 10 m above the ground surface transformed from the wind profile power law are 2.2 m s^{-1} and 17.7 m s^{-1} .

Thus, the classification criteria of SWS are based on two aspects: (1) the cut-in and cut-out wind speeds defining the range of efficient SWS used in power generation; (2) the incrementing percentiles of SWS among efficient SWS. The incrementing percentiles refer to the values of 50th, 60th, 70th, 80th, and 90th corresponding to 2.9 m s^{-1} , 3.5 m s^{-1} , 4.1 m s^{-1} , 5.0 m s^{-1} , and 6.2 m s^{-1} . These values are obtained by averaging values for 41 years and over global stations aiming to set a uniform standard of categorization. At the same time, we consider zero SWS into one separate group to verify the result of data correction (Dunn et al 2022a) and describe small wind speeds more accurately. Then SWS data was divided into nine ranges to show the changes in the SWS frequency at different ranges (table 1). We denote SWS in specific range i as class i ($i = 1, 2, \dots, 9$, table 1). Here, SWS of class 3–8 is efficient wind speed.

2.2.3. Quantification of the influence of the SWS frequency variation

To validate the categorization, we use the Pearson correlation coefficient to compare the SWS from *in-situ* data and weighted-average speed calculated by the following formula:

$$\text{Weighted}_v(t) = \sum_{i=1}^9 \bar{v}_i f_i(t) \tag{2}$$

where \bar{v} is the climatological mean of SWS of the corresponding wind speed category over 41 years (all the subscripts indicated the wind speed range),

$\text{Weighted}_v(t)$ and $f_i(t)$ are the wind speed and frequency of year t accordingly.

To estimate the contribution of SWS frequency changes of each class to the wind speed trend, we keep the multiplication of frequency and mean SWS in a specific class of SWS to be a constant value as the 41 year climatology mean value, denoted as $\bar{v}_i f_i$, to calculate the fixed weighted-average SWS (Fixed_{v_i}) within class i :

$$\text{Fixed}_{v_i}(t) = \text{Weighted}_v(t) - \bar{v}_i f_i(t) + \bar{v}_i f_i. \tag{3}$$

The difference (Diff_{v_i}) between the weighted-average speed (Weighted_v) and fixed weighted-average SWS (Fixed_{v_i}) representing the influence of the certain range of SWS to the weighted-average wind speed, as shown in formula (4):

$$\begin{aligned} \text{Diff}_{v_i}(t) &= \text{Weighted}_v(t) - \text{Fixed}_{v_i}(t) \\ &= \bar{v}_i f_i(t) - \bar{v}_i f_i. \end{aligned} \tag{4}$$

We calculate the ratio of the trend of Diff_{v_i} to the trend of Weighted_v according to the following formula (5) representing the contributions of changes of frequency in each class to the general changes of weighted-average SWS:

$$\begin{aligned} \frac{\partial \text{Weighted}_v}{\partial t} &= \sum_{i=1}^9 \bar{v}_i \frac{\partial f_i(t)}{\partial t} = \sum_{i=1}^9 \frac{\partial (\bar{v}_i f_i(t) - \bar{v}_i f_i)}{\partial t} \\ &= \sum_{i=1}^9 \frac{\partial \text{Diff}_{v_i}}{\partial t}. \end{aligned} \tag{5}$$

The trend of weighted SWS is the sum of the trends of the nine classes of Diff_{v_i} , thus having little chance to be close to zero as the denominator. The trend of Diff_{v_i} is dependent on the only variable frequency $f_i(t)$. In this way, for SWS at each class i , the trend of Diff_{v_i} ends up to be a proportion of the trend of Weighted_v .

2.2.4. Wind power assessment

The theoretical power assessment of wind turbines requires complex parameters such as air density and turbine parameters, which introduces vast complexity to set influencing parameters properly (Sohoni et al 2016), especially when considering the global spatial extent of our study. The power curve of wind turbines is helpful for wind energy forecasting without further technical details of wind power operating conditions (Lydia et al 2014). It is widely used in wind power assessment (Wang et al 2016,

Pryor *et al* 2020, Millstein *et al* 2022). We assume the wind turbine GE 2.5-120 was installed around each observation site and use its power curve to derive the wind power output under the wind regime at observation sites. Wind turbines at higher hub heights tend to experience better wind regimes with stronger wind and generate more energy (Yang *et al* 2018). In this research, we considered hub heights of 110 m and 139 m to ensure that the results are comprehensive and convincing. Yearly wind power generation (Energy, unit: GW·h) is calculated by combining the global wind turbine installations and the capacity factor based on formula (6), that is, the ratio of wind power output (P_{real} , unit: MW) to rated power ($P_{\text{rated}} = 2.5$ MW) multiplied by the installed capacity (837 GW). Installed capacity data is from the Global Wind Energy Council (2022),

$$\text{Energy} = \text{Capacity} \times \frac{P_{\text{real}}}{P_{\text{rated}}} \times 365 \times 24. \quad (6)$$

3. Results and discussion

3.1. Wind speed changes

We found that global SWS in the corrected HadISD showed a continuous decline during 1980–2010 with a rate of $-0.08 \text{ m s}^{-1} \text{ decade}^{-1}$ ($p < 0.001$). The turning year was near 2010, and then SWS increased at a rate of $0.096 \text{ m s}^{-1} \text{ decade}^{-1}$ ($p < 0.001$, figure 1(a)). At the continental scale, the changes in SWS from 1980 to around 2010 varied and turning points marking the different SWS trends are found in most continents except for Africa. In North America, Europe and Asia, a turning point marking the declining trend transferring to an increasing trend can be identified (figures 1(b)–(d)). The declining SWS trends in America and Europe were close, with $-0.118 \text{ m s}^{-1} \text{ decade}^{-1}$ and $-0.112 \text{ m s}^{-1} \text{ decade}^{-1}$ (both $p < 0.001$), respectively. The slowing down of SWS was faster in Asia, with a trend of $-0.136 \text{ m s}^{-1} \text{ decade}^{-1}$ ($p < 0.001$). Moreover, the turning point indicating the wind speed reversal occurred early in 2000 in Asia, for example, in southwestern China (Xiaomei *et al* 2012). While in Europe and North America, the turning points occurred later in 2012 and 2010, respectively. From 2011 to 2021, the reversed increasing trends of SWS in North America and Europe were not significant, being respectively $0.084 \text{ m s}^{-1} \text{ decade}^{-1}$ ($p > 0.05$), $0.056 \text{ m s}^{-1} \text{ decade}^{-1}$ ($p > 0.05$), while the trend in Asia is $0.091 \text{ m s}^{-1} \text{ decade}^{-1}$ ($p < 0.001$). The asymmetry between the SWS weakening trend and the SWS reversal trend is consistent with the previous studies (Wu *et al* 2018, Zeng *et al* 2019, Deng *et al* 2021, Liu *et al* 2022). Exploring the trends of SWS aids in the comprehensive analysis of SWS frequency variation.

On the other hand, SWS in South America, Africa, and Australia did not show the first weakening and then reversing trend. The SWS in South America

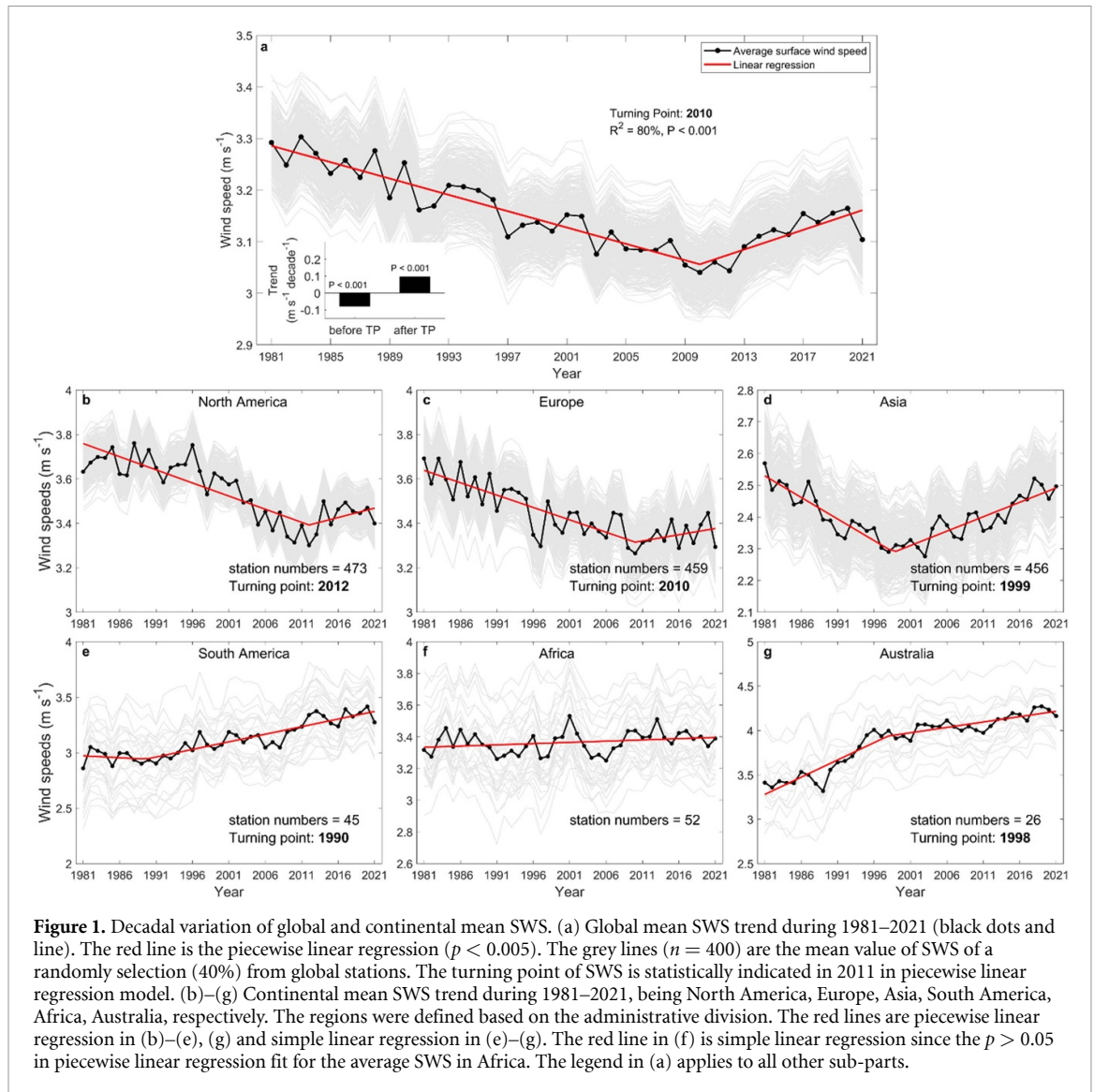
has a nonsignificant trend before 1990 ($p > 0.05$), then following a continuous increasing trend with a rate of $0.14 \text{ m s}^{-1} \text{ decade}^{-1}$ ($p < 0.05$) till 2021 (figure 1(e)). Yet, neither an increase nor decrease trend of SWS is found in Africa ($p > 0.05$, figure 1(f)). The SWS in Australia first increases at a rate of $0.39 \text{ m s}^{-1} \text{ decade}^{-1}$ ($p < 0.05$) during 1981–1998, then such increase slows down after 1998 with a rate of $0.12 \text{ m s}^{-1} \text{ decade}^{-1}$ ($p < 0.05$, figure 1(g)). The SWS trend from *in-situ* observations in the Southern Hemisphere remains highly uncertain, which may be due to the lack of enough long-term observations, relocation of *in-situ* stations or changes in the observational practices (Lucas 2010, Wu *et al* 2018). For instance, the increasing trend of SWS was found in Australia based on the observations from 14 stations during 1975–2006 (Troccoli *et al* 2012). Meanwhile, a decreasing trend of SWS is found using observations from 163 stations for the same period (McVicar *et al* 2008).

3.2. Frequency changes of global and regional SWS

Wind speed trends are closely associated with frequency. We found that the wind speed distribution had changed during the past decades (figure 2(a)), implying the frequency change at different SWS categories. Notably, 90th SWS has been decreased from 6.6 m s^{-1} to 6.2 m s^{-1} from 1982 to 2021, indicating that the SWS frequency tends to increase and centralize in relatively small winds from 1 to 3 m s^{-1} (figure 2(a)). Moreover, the peak of the wind speed distribution shifts towards smaller values as time passes (figure 2(a)), implying an increase in the skewness in SWS frequency. A similar increase of skewness and kurtosis of SWS distribution was found during 2006–2019, as was predicted in 2020–2099 under the representative concentration pathway RCP8.5 (Jung and Schindler 2019a).

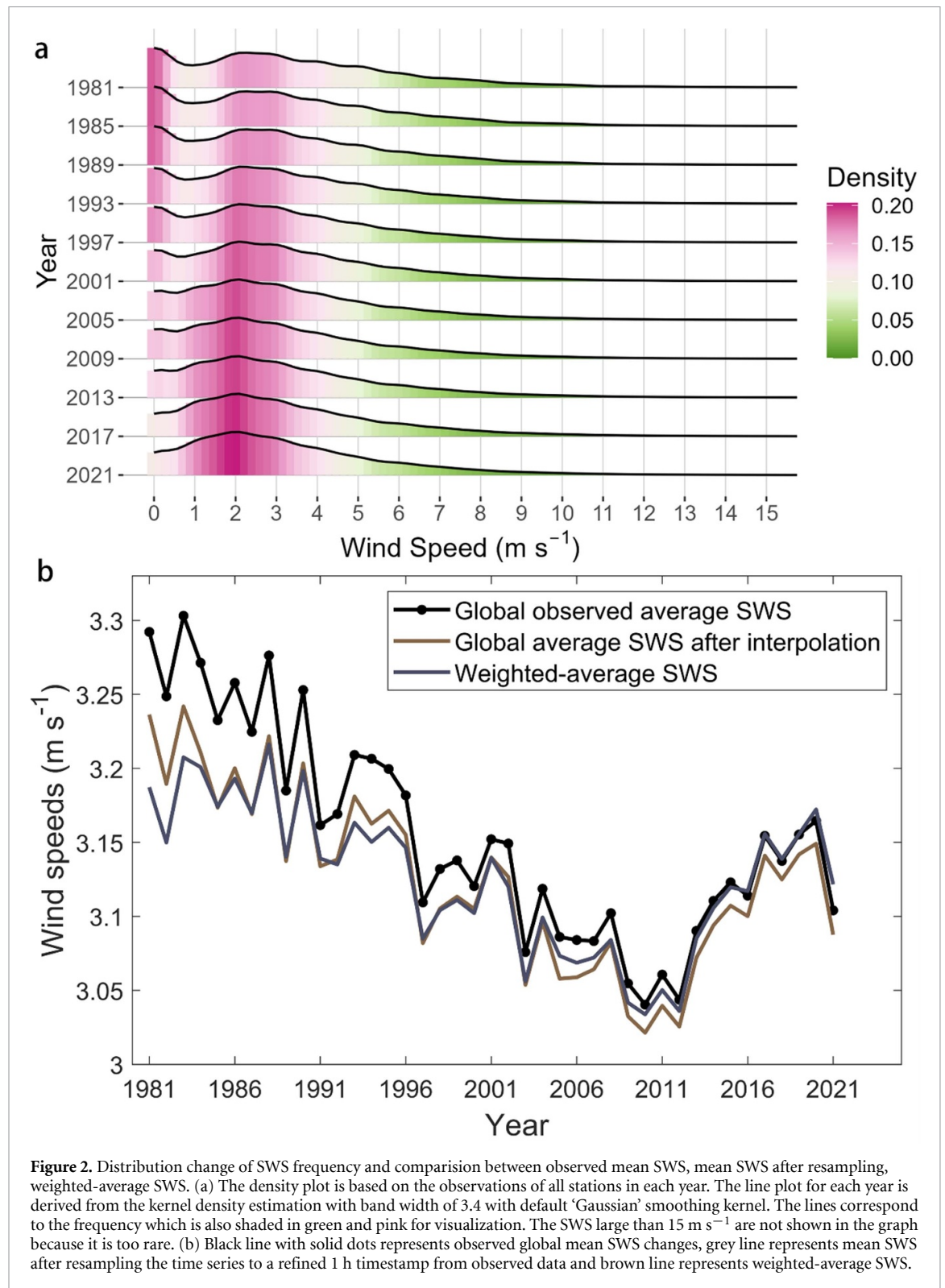
After the SWS resampling, resampled SWS was divided into nine ranges based on the positive-skewed wind speed distribution and contribution to wind energy generation (see section 2.2). To validate the categorization of SWS, the weighted-average SWS calculated from formula (2) was compared with the observed mean SWS after resampling (figure 2(b)). The Pearson correlation coefficient of weighted-average SWS and the observed average was 0.998 ($p < 0.01$; figure S7), implying that the classification criteria of SWS categorization were rather satisfying. Notice, however, that there was a slight deviation between the weighted-average SWS and the observed SWS. This was because we used the climatological mean value of SWS to multiply the changing frequency when calculating weighted-average SWS.

The change in SWS frequency during the past decades is shown in figure 3. Calm wind frequency decreased ($-2.61\% \text{ decade}^{-1}$, $p < 0.001$) for the past 41 years (figure 3(a)). An increase with a rate of 3.47%



decade⁻¹ ($p < 0.001$) was found in class 2 (0.1–2.1 m s⁻¹) wind frequency (figure 4(b)). However, the class 2 wind was smaller than the cut-in wind speed and thus did not contribute to the wind power generation. The frequency of class 9 (> 17.7 m s⁻¹) wind was so small that the decrease rate was only -0.01% decade⁻¹ ($p < 0.001$). Up to 60% of wind speed records fall in class 3–8 that can be used for wind power generation (figures 3(c)–(h)). Among them, SWS frequency at class 3 and class 5 increased at a rate of 0.18% decade⁻¹ and 0.37% decade⁻¹ (both $p < 0.001$, figures 3(c) and (e)), while SWS frequency at class 7 and class 8 decreased at a rate of -0.71% decade⁻¹ and -0.68% decade⁻¹ (both $p < 0.001$, figures 3(g) and (h)). increase in wind speed frequency mainly occurred for relatively low winds, we suggest that the reversal of global SWS was attributed to the decreasing frequency of calm winds and the increasing frequency of light winds. However, light winds are generally smaller than v_i (2.2 m s⁻¹), which has a limited effect on promoting wind power generation (Pryor and Barthelmie 2010).

The decreasing frequency of relatively strong wind is noteworthy because a majority of wind power generation depends on the strong SWS (Tian et al 2019). To quantify the influence of the changing SWS frequency on wind speed trend, we combined the frequency with climatological mean SWS at each class. Regarding a significant turning point around 2010, the trend of Diff_v is analyzed separately in 1981–2010 and 2011–2021. During 1981–2010, a substantial change is found in class 2, class 7, and class 8 (figure 4(a)). The Diff_v at class 2 had significantly increased at a rate of 5.82% m s⁻¹ decade⁻¹ ($p < 0.001$), meaning that the increase in class 2 wind contributes 99.94% to offset part of the global wind stilling trend (figure 4(b), table 2). Nevertheless, the Diff_v at class 7 and class 8 decreased by -4.90% m s⁻¹ decade⁻¹ and -6.85% m s⁻¹ decade⁻¹ ($p < 0.001$), respectively, meaning that the decrease in class 7 and class 8 winds contributed 89.00% and 124.52% to the wind stilling (figure 4(b), table 2). After 2011, almost SWS in all classes has positive contribution to wind speed



reversal, but the contribution of slight wind (class 2–3) are larger, accounting for 33.17%, 30.90% respectively for class 2, 3. Since the strong winds of class 7 and class 8 had an apparent trend change from $-11.50\% \text{ m s}^{-1} \text{ yr}^{-1}$ ($p < 0.001$, 1981–2010) to an increased rate of $3.00\% \text{ m s}^{-1} \text{ yr}^{-1}$ ($p < 0.001$, 2011–2020), they had the largest contribution (i.e. 73.38%) to the trend changes of average SWS from stilling state to reversal state. The substantial decrease of strong

winds during 1981–2010 and slight increase with fluctuation during 2011–2021 concurs with the results of Dunn *et al* (2022b). Here, the Diff, in figure 4(a) is always zero because class 1 only contains calm wind, though the frequency of calms does show variations.

Regionally, the calm wind frequency in Asia and South America decreased from over 25% to below 10% from 1990 to 2010 (figure 5(a)). The decrease was smaller for Africa, Australia and Europe

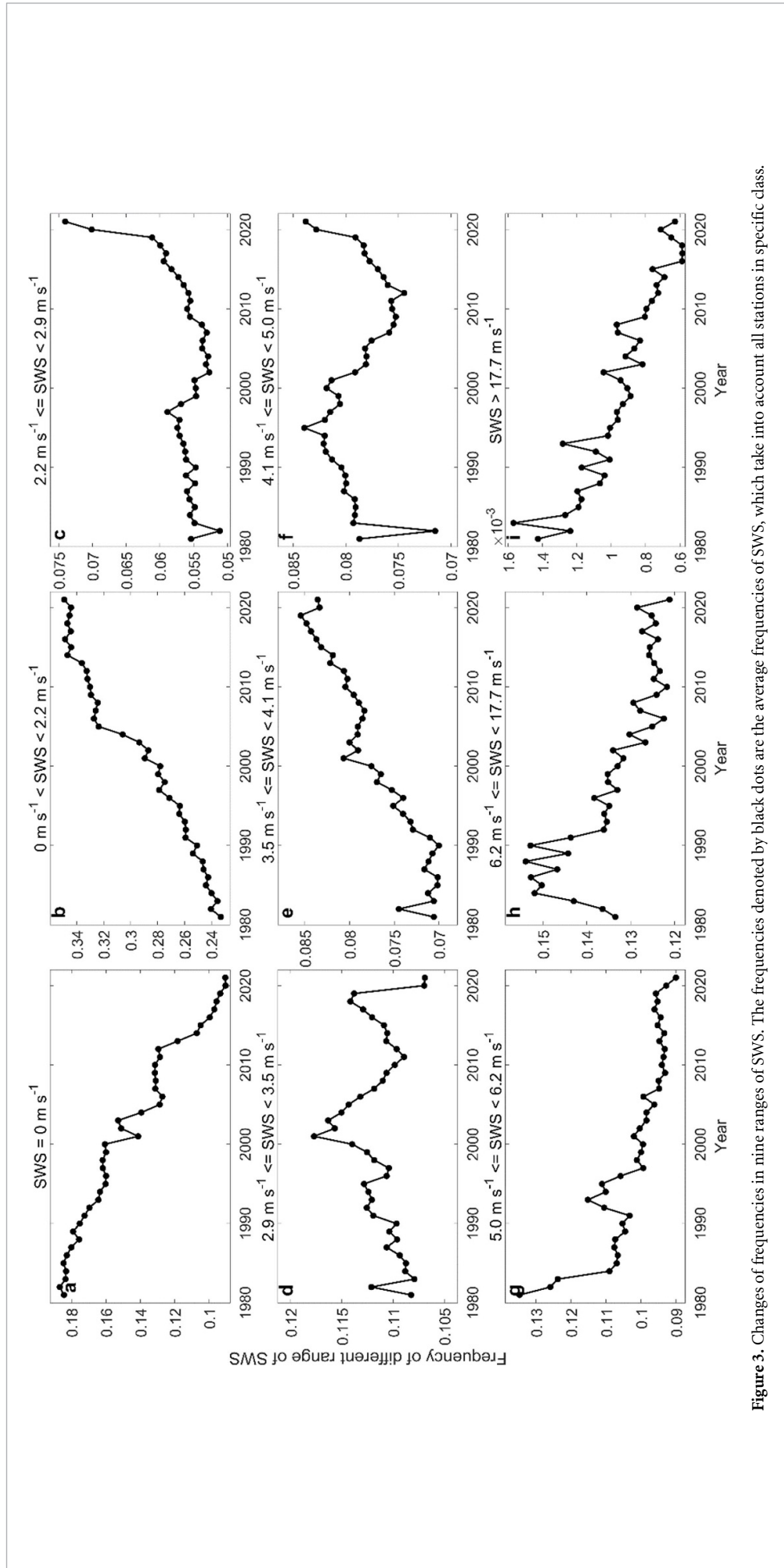


Figure 3. Changes of frequencies in nine ranges of SWS. The frequencies denoted by black dots are the average frequencies of SWS, which take into account all stations in specific class.

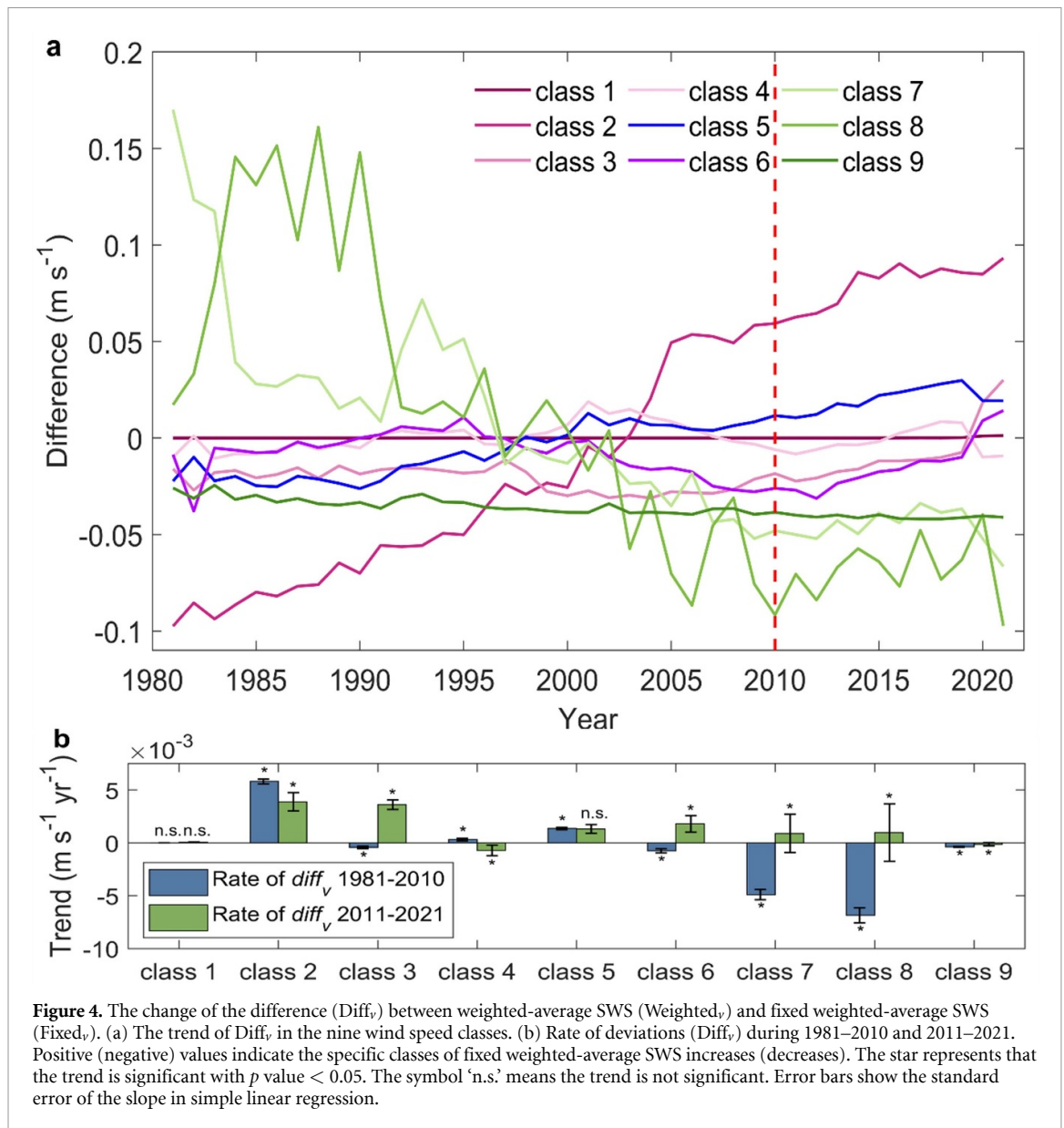


Figure 4. The change of the difference ($Diff_v$) between weighted-average SWS ($Weighted_v$) and fixed weighted-average SWS ($Fixed_v$). (a) The trend of $Diff_v$ in the nine wind speed classes. (b) Rate of deviations ($Diff_v$) during 1981–2010 and 2011–2021. Positive (negative) values indicate the specific classes of fixed weighted-average SWS increases (decreases). The star represents that the trend is significant with p value < 0.05 . The symbol ‘n.s.’ means the trend is not significant. Error bars show the standard error of the slope in simple linear regression.

Table 2. The rate of $Diff_v$ and the contribution to weighted-average SWS changes. The rate of $Diff_v$ is calculated before 2010 (i.e. 1980–2010) and after 2011 (i.e. 2011–2021) for each wind speed class. The trend of $Diff_v$ at class 1 is not shown due to that class 1 only contains SWS = 0 m s⁻¹, resulting in $Diff_v$ is always zero though the frequency of calm wind changes.

| | Trend of $Diff_v$ before 2011 (m s ⁻¹ decade ⁻¹) | Contribution percentage | Trend of $Diff_v$ after 2011 (m s ⁻¹ decade ⁻¹) | Contribution percentage |
|---------|---|-------------------------|--|-------------------------|
| Class 2 | 5.82% | -99.94% | 3.88% | 33.17% |
| Class 3 | -0.43% | 7.89% | 3.61% | 30.90% |
| Class 4 | 0.31% | -5.67% | -0.71% | -5.95% |
| Class 5 | 1.36% | -24.78% | 1.32% | 11.00% |
| Class 6 | -0.75% | 13.72% | 1.80% | 15.00% |
| Class 7 | -4.90% | 89.00% | 0.89% | 7.44% |
| Class 8 | -6.85% | 124.52% | 0.97% | 8.08% |
| Class 9 | -0.38% | 6.85% | -0.13% | -1.10% |

(figure 5(a)). Calm wind frequency did not show a noticeable change in North America, instead having significant interannual variations. In Asia, most winds were found to be the light wind of class 2, and the frequency of class 2 wind reached over 50% in 2005–2021 (figure 5(b)). South America and

Europe has the largest increment in the frequency of moderate wind (class 3–6), which increased from 29.48% and 29.44% in 1981 to 41.46% and 42.37% in 2021 (figures 5 (c)–(f)). The frequency of moderate wind has no apparent change in North America and Europe for 41 years. Australia is an exception for

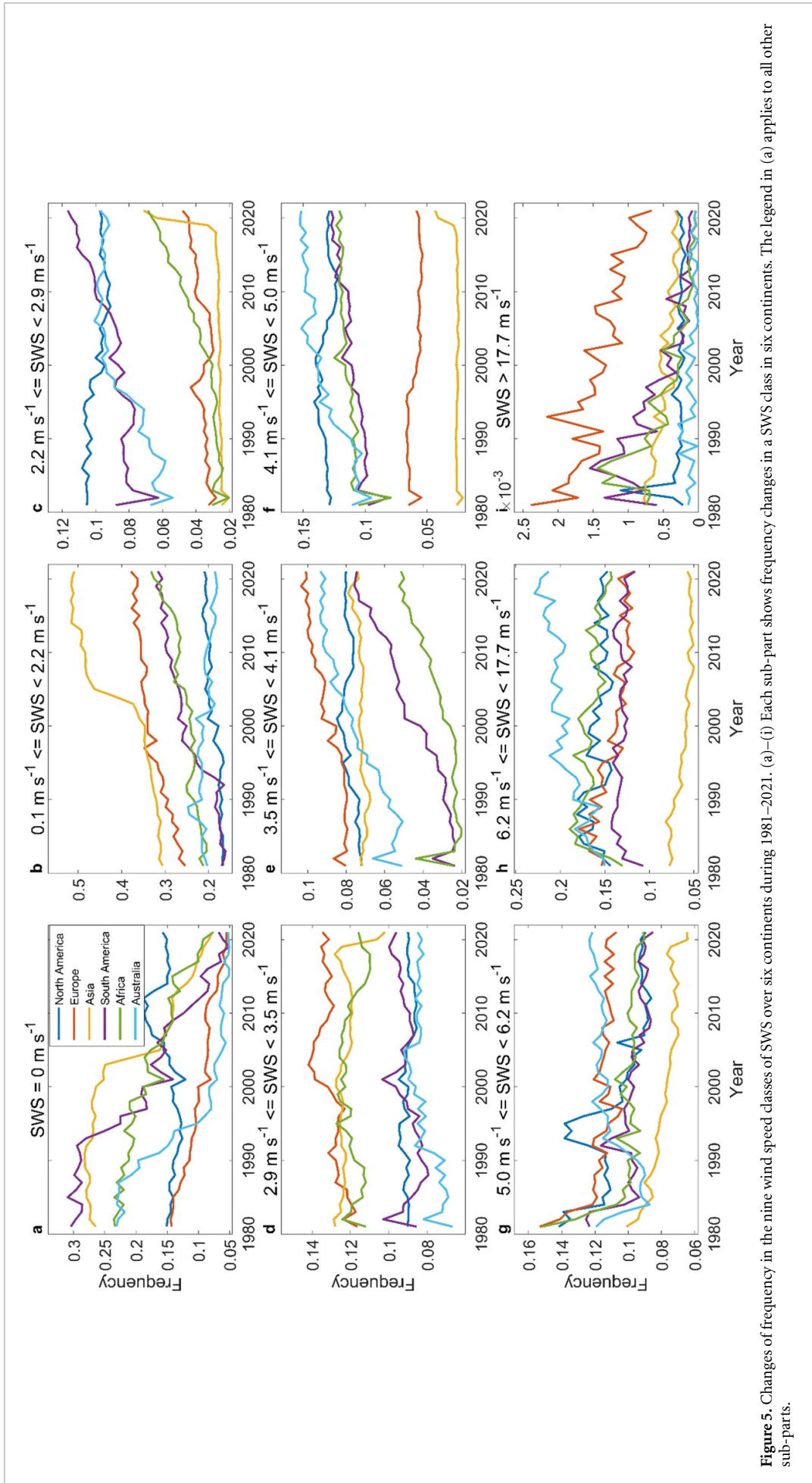
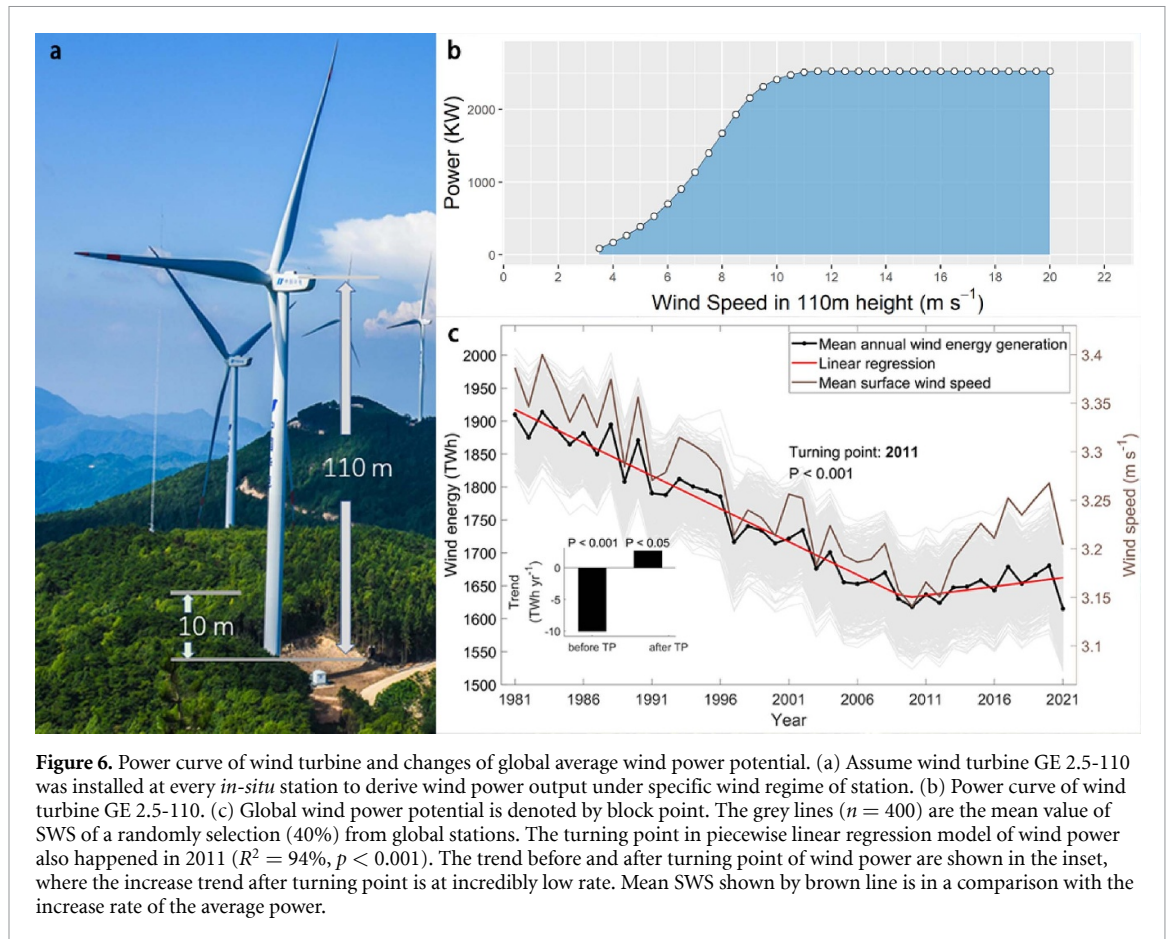


Figure 5. Changes of frequency in the nine wind speed classes of SWS over six continents during 1981–2021. (a)–(i) Each sub-part shows frequency changes in a SWS class in six continents. The legend in (a) applies to all other sub-parts.



the observed increasing frequency of strong wind at classes 6–8, yet this is obtained by only 26 stations (figures 5(f)–(h)). As for the class 9 wind frequency, a consistent decrease is found in nearly all continents (figure 5(i)). This rapid decrease in strong wind concurs with a series of earlier regional studies conducted in America (Pryor *et al* 2007, 2009), China (Guo *et al* 2011, Zha *et al* 2017), Central Asia (Dunn *et al* 2022b), the United Kingdom (Earl *et al* 2013) and Spain and Portugal (Azorin-Molina *et al* 2016).

3.3. Effect of wind speed frequency change on wind power potential

To understand the role of continuously decreasing strong winds in wind energy generation, we made an effort to quantify the above results in terms of wind power generation potential both at global and continental scales without considering the influence of technological improvement. Based on global wind power capacity in 2021 (837 GW) and the power curve of wind turbine GE 2.5-120 at 110 m hub height, the wind energy was estimated to have a continued decline with a rate of $-10.02 \text{ TWh yr}^{-1}$ ($p < 0.001$) during 1981–2010, and then a reversal with a rate of 2.67 TWh yr^{-1} ($p < 0.05$) during 2011–2021 (figure 6(c)). Wind energy was generally larger than 100 TWh when the hub height was 139 m, with decreasing trend of $10.36 \text{ TWh yr}^{-1}$ ($p < 0.001$) during 1981–2010 and an increasing

trend of 2.95 TWh yr^{-1} ($p < 0.05$) during 2011–2021 (appendix figure S8), which suggested that hub height has a little impact on trend changes of wind energy. The wind energy mentioned below is all based on hub height = 110 m. Compared to the reversal trend of SWS, the recovery of wind power is much slighter. Re-analysis data also report no noticeable changes in mean annual global wind energy generation (Jung *et al* 2019b). Wind power's reversal trend is relatively weak due to the decline in strong wind frequency.

The wind power changes are quite different from the trend of SWS in Asia and Africa. After a substantial decrease trend ($-6.29 \text{ TWh yr}^{-1}$, $p < 0.05$), the wind power was still decrease ($-0.79 \text{ TWh yr}^{-1}$, $p < 0.05$) after the turning year of SWS in Asia, since the rebound of SWS mainly driven by the small wind at class 2 (figure 5(b)). Wind power in Africa also decreased in the past decade with a rate of $-0.001 \text{ TWh yr}^{-1}$ ($p < 0.05$, figure 7(e)). Tian *et al* (2019) also reported a decline in wind power potential in half of the stations in Africa. For other continents, the decreasing rates of wind power in America and Europe were $-2.06 \text{ TWh yr}^{-1}$ and $-3.31 \text{ TWh yr}^{-1}$ ($p < 0.001$) before turning years of SWS. After the turning years, the increasing rates were only 0.86 TWh yr^{-1} and 0.76 TWh yr^{-1} . Studies have also shown a slow increase in average wind energy in the United States over the last decades (Jung *et al*

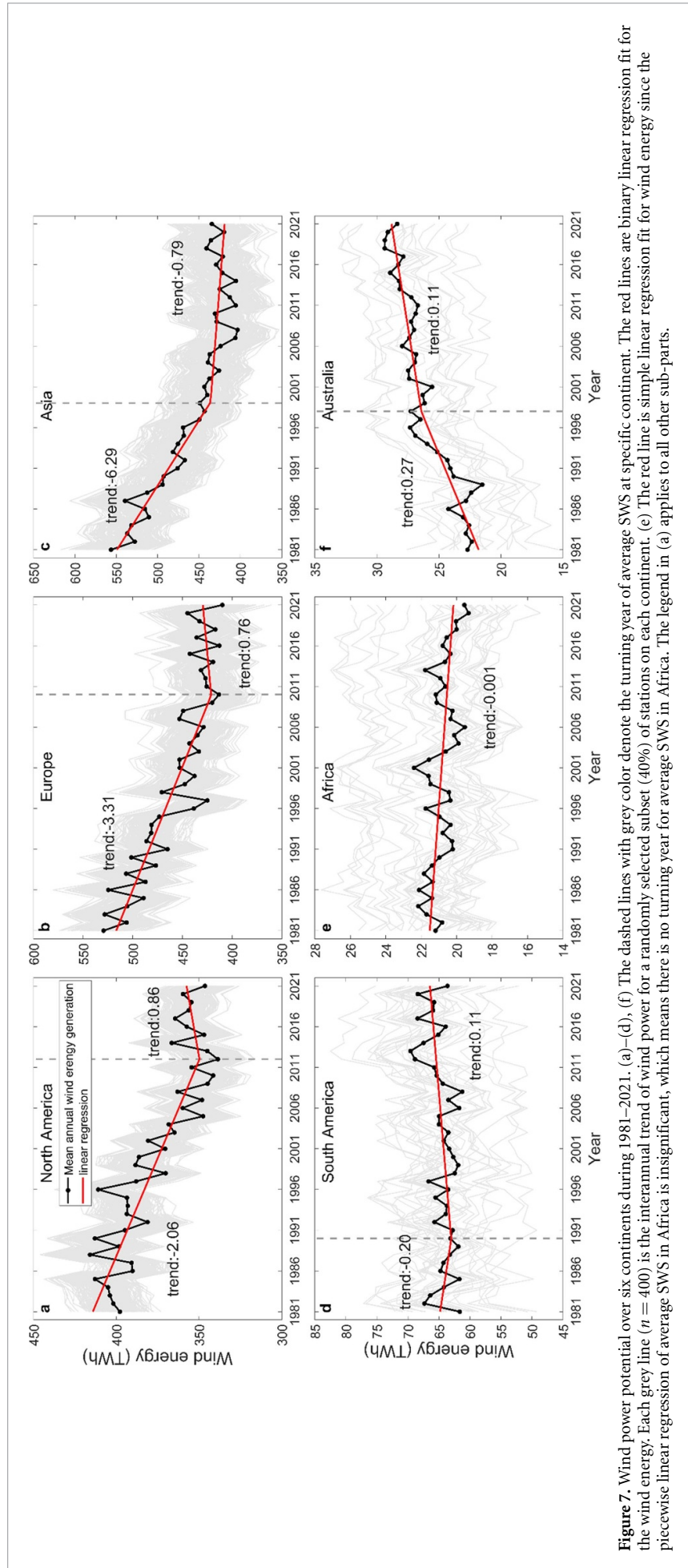


Figure 7. Wind power potential over six continents during 1981–2021. (a)–(d), (f) The dashed lines with grey color denote the turning year of average SWS at specific continent. The red lines are binary linear regression fit for the wind energy. Each grey line ($n = 400$) is the interannual trend of wind power for a randomly selected subset (40%) of stations on each continent. (e) The red line is simple linear regression fit for wind energy since the piecewise linear regression of average SWS in Africa is insignificant, which means there is no turning year for average SWS in Africa. The legend in (a) applies to all other sub-plots.

2019b). Australia and South America still maintained increasing trends of wind power during 1981–2021, both with comparable rates of 0.11 TWh yr^{-1} after the turning years (figures 7(d) and (f)). Overall, the increase in wind power after the turning point of SWS was not as strong as the reversal of SWS in the recent decade for the reason that the weakening of strong winds hinders the upward trajectory of the global wind energy industry.

Other factors may affect our analysis of wind power assessment. The atmospheric stability and topography (e.g. mountainous and coastal regions) can affect wind power generation by shaping the main parameter α in the power law (Pryor *et al* 2020, Pacheco de Sá Sarmiento *et al* 2022), while we assume a constant and homogenous α in calculation. In addition, the wake effect in wind farms can also be an important factor. It has been suggested that the wake effect cause an average energy loss of around 5.8% in downwind wind farms (Wang *et al* 2022a, 2022b). Given our estimation does not consider the wake effects, thus our wind energy analysis may overestimate the global power potential. Although there are still uncertainties, this study offers a broad and worldwide estimate; meanwhile, more detailed regional assessments of wind energy help quantify the impact of continuing strong wind declines and benefit investment decisions.

4. Conclusion

We conducted a global spatiotemporal analysis on the variation of SWS trend and SWS frequency in recent decades (i.e. 1981–2021) and evaluated its impact on wind power generation. Analysis of wind speed frequencies emphasized that the decrease of strong wind frequency ($\text{SWS} > 5.0 \text{ m s}^{-1}$) is a dominant cause of wind stilling with a contribution of 215.96%. After the turning year of 2010, the continuous increase of the light wind ($0.1 \text{ m s}^{-1} < \text{SWS} < 2.9 \text{ m s}^{-1}$) accompanying the decreasing calm wind mainly contributes 63.65% to wind speed reversal. Notably, the continuous increase in the frequency of light wind made a negligible contribution to wind power generation. Therefore, the rise in wind power potential was not as optimistic as subjectively estimated based on the reversal trend of average SWS. Global mean annual wind power potential only showed a slight increase at a rate of 2.67 TWh yr^{-1} ($p < 0.05$) from 2011 to 2021 (the 1981–2010 rate was $-10.02 \text{ TWh yr}^{-1}$, $p < 0.001$) compared to the substantial reversal of mean SWS at $0.09 \text{ m s}^{-1} \text{ decade}^{-1}$ ($p < 0.001$) over 2011–2021 (the 1981–2010 rate is $-0.08 \text{ m s}^{-1} \text{ decade}^{-1}$, $p < 0.001$) of mean SWS.

Several issues deserve further research: firstly, synoptic phenomena like wind gusts (e.g. 3 s maximum wind speed) are not included in our results and discussions as the dataset used do not have the

higher temporal resolution needed for their study. Secondly, the cause(s) of the continuously decreasing strong wind is yet to be fully explored and understood. Finally, finer-scale regional assessments of wind energy can help supplement the uncertainties associated with large-scale assessments, taking into account the effects of atmospheric stability and topography.

Data availability statement

The data that support the findings of this study are openly available at the following URL/DOI: www.metoffice.gov.uk/hadobs/hadis/.

Acknowledgments

This study was supported by the National Natural Science Foundation of China (Grant No. 42071022), Guangdong Basic and Applied Basic Research Fund (2022A1515240070) and the start-up fund provided by Southern University of Science and Technology (no. 29/Y01296122). C A-M was supported by the IBER-STILLING (RTI2018-095749-A-I00, MCIU/AEI/FEDER,UE); VENTS (GVA-AICO/2021/023); the CSIC Interdisciplinary Thematic Platform (PTI) Clima (PTI-CLIMA); and the 2021 Leonardo Grant for Researchers and Cultural Creators, BBVA Foundation. RJHD was supported by the Met Office Hadley Centre Climate Programme funded by BEIS and by the UK-China Research & Innovation Partnership Fund through the Met Office Climate Science for Service Partnership (CSSP) China as part of the Newton Fund. SJ was supported by the Ramon y Cajal program and the OPEN project (RYC2020-029993-I and TED2021-131074B-I00, MCIU/AEI/FEDER,UE). All the specific country observational organizations who establish, maintain, and run observational networks are the fundamental to the global ISD and HadISD databases.

Author contributions


Zhenzhong Zeng: Conceptualization, Methodology
Yanan Zhao: Methodology, Software, Writing—Draft
All other authors: Writing—Review & Editing.

ORCID iDs

Yanan Zhao  <https://orcid.org/0009-0006-7766-6005>

Shijing Liang  <https://orcid.org/0000-0001-8136-484X>

Yi Liu  <https://orcid.org/0000-0002-5515-8804>

Tim R McVicar  <https://orcid.org/0000-0002-0877-8285>

Cesar Azorin-Molina  <https://orcid.org/0000-0001-5913-7026>
 Robert J H Dunn  <https://orcid.org/0000-0003-2469-5989>
 Sonia Jerez  <https://orcid.org/0000-0002-2153-1658>
 Xinrong Yang  <https://orcid.org/0000-0001-9469-9884>

References

- Azorin-Molina C, Guijarro J-A, McVicar T R, Vicente-Serrano S M, Chen D, Jerez S and Espirito-Santo F 2016 Trends of daily peak wind gusts in Spain and Portugal, 1961–2014 *J. Geophys. Res. Atmos.* **121** 1059–78
- Deng K, Azorin-Molina C, Minola L, Zhang G and Chen D 2021 Global near-surface wind speed changes over the last decades revealed by reanalyses and CMIP6 model simulations *J. Clim.* **34** 2219–34
- Dunn R J H et al 2022b Global climate *Bull. Am. Meteorol. Soc.* **103** S11–142
- Dunn R J H, Azorin-Molina C, Menne M J, Zeng Z, Casey N W and Shen C 2022a Reduction in reversal of global stilling arising from correction to encoding of calm periods *Environ. Res. Commun.* **4** 061003
- Dunn R J H, Willett K M, Morice C P and Parker D E 2014 Pairwise homogeneity assessment of HadISD *Clim. Past* **10** 1501–22
- Dunn R J H, Willett K M, Parker D E and Mitchell L 2016 Expanding HadISD: quality-controlled, sub-daily station data from 1931 *Geosci. Instrum. Methods Data Syst.* **5** 473–91
- Earl N, Dorling S, Hewston R and Glasow R V 2013 1980–2010 variability in U.K. surface wind climate *J. Clim.* **26** 1172–91
- Eurek K, Sullivan P, Gleason M, Hettlinger D, Heimiller D and Lopez A 2017 An improved global wind resource estimate for integrated assessment models *Energy Econ.* **64** 552–67
- Global Wind Energy Council 2022 Global wind report 2022 (Brussels: Global Wind Energy Council) (available at: <https://gwec.net/global-wind-report-2022/>)
- Guo H, Xu M and Hu Q 2011 Changes in near-surface wind speed in China: 1969–2005 *Int. J. Climatol.* **31** 349–58
- International Energy Agency (IEA) 2020 World energy outlook 2020 (OECD Publishing) (available at: www.iea.org/reports/world-energy-outlook-2020)
- Islam M R, Saidur R and Rahim N A 2011 Assessment of wind energy potentiality at Kudat and Labuan, Malaysia using Weibull distribution function *Energy* **36** 985–92
- Jung C and Schindler D 2019a Changing wind speed distributions under future global climate *Energy Convers. Manage.* **198** 111841
- Jung C, Taubert D and Schindler D 2019b The temporal variability of global wind energy—long-term trends and inter-annual variability *Energy Convers. Manage.* **188** 462–72
- Liu F, Sun F, Liu W, Wang T, Wang H, Wang X and Lim W H 2019 On wind speed pattern and energy potential in China *Appl. Energy* **236** 867–76
- Liu Y et al 2022 Increases in China's wind energy production from the recovery of wind speed since 2012 *Environ. Res. Lett.* **17** 114035
- Lucas C 2010 On developing a historical fire weather data-set for Australia *Aust. Meteorol. Oceanogr. J.* **61** 1–13
- Lydia M, Kumar S S, Selvakumar A I and Prem Kumar G E 2014 A comprehensive review on wind turbine power curve modeling techniques *Renew. Sustain. Energy Rev.* **30** 452–60
- McElroy M B, Lu X, Nielsen C P and Wang Y 2009 Potential for wind-generated electricity in China *Science* **325** 1378–80
- McVicar T R et al 2012 Global review and synthesis of trends in observed terrestrial near-surface wind speeds: implications for evaporation *J. Hydrol.* **416–417** 182–205
- McVicar T R, Van Niel T G, Li L T, Roderick M L, Rayner D P, Ricciardulli L and Donohue R J 2008 Wind speed climatology and trends for Australia, 1975–2006: capturing the stilling phenomenon and comparison with near-surface reanalysis output *Geophys. Res. Lett.* **35** L20403
- Millstein D, Bolinger M and Wiser R 2022 What can surface wind observations tell us about interannual variation in wind energy output? *Wind Energy* **25** 1142–50
- Pacheco de Sá Sarmiento F I, Goes Oliveira J L and Passos J C 2022 Impact of atmospheric stability, wake effect and topography on power production at complex-terrain wind farm *Energy* **239** 122211
- Pryor S C and Barthelmie R J 2010 Climate change impacts on wind energy: a review *Renew. Sustain. Energy Rev.* **14** 430–7
- Pryor S C, Barthelmie R J, Bukovsky M S, Leung L R and Sakaguchi K 2020 Climate change impacts on wind power generation *Nat. Rev. Earth Environ.* **1** 627–43
- Pryor S C, Barthelmie R J and Riley E S 2007 Historical evolution of wind climates in the USA *J. Phys.: Conf. Ser.* **75** 012065
- Pryor S C, Barthelmie R J, Young D T, Takle E S, Arritt R, WFlory D, Gutowski W J Jr, Nunes A and Roads J 2009 Wind speed trends over the contiguous United States *J. Geophys. Res. Atmos.* **114** D14
- Roderick M L, Rotstayn L D, Farquhar G D and Hobbins M T 2007 On the attribution of changing pan evaporation *Geophys. Res. Lett.* **34**
- Smith A, Lott N and Vose R 2011 The integrated surface database: recent developments and partnerships *Bull. Am. Meteorol. Soc.* **92** 704–8
- Sohoni V, Gupta S C and Nema R K 2016 A critical review on wind turbine power curve modelling techniques and their applications in wind based energy systems *J. Energy* **2016** e8519785
- Tian Q, Huang G, Hu K and Niyogi D 2019 Observed and global climate model based changes in wind power potential over the northern Hemisphere during 1979–2016 *Energy* **167** 1224–35
- Troccoli A, Muller K, Coppin P, Davy R, Russell C and Hirsch A L 2012 Long-term wind speed trends over Australia *J. Clim.* **25** 170–83
- Vautard R, Cattiaux J, Yiou P, Thépaut J-N and Ciais P 2010 Northern Hemisphere atmospheric stilling partly attributed to an increase in surface roughness *Nat. Geosci.* **3** 756–61
- Wang J, Hu J and Ma K 2016 Wind speed probability distribution estimation and wind energy assessment *Renew. Sustain. Energy Rev.* **60** 881–99
- Wang Q, Luo K, Wu C, Mu Y, Tan J and Fan J 2022a Diurnal impact of atmospheric stability on inter-farm wake and power generation efficiency at neighboring onshore wind farms in complex terrain *Energy Convers. Manage.* **267** 115897
- Wang Q, Luo K, Wu C, Zhu Z and Fan J 2022b Mesoscale simulations of a real onshore wind power base in complex terrain: wind farm wake behavior and power production *Energy* **241** 122873
- Woolway R I, Merchant C J, Van Den Hoek J, Azorin-Molina C, Nôges P, Laas A, Mackay E B and Jones I D 2019 Northern Hemisphere atmospheric stilling accelerates lake thermal responses to a warming world *Geophys. Res. Lett.* **46** 11983–92
- Wu J, Zha J, Zhao D and Yang Q 2018 Changes in terrestrial near-surface wind speed and their possible causes: an overview *Clim. Dyn.* **51** 2039–78
- Xiaomei Y, Zongxing L, Qi F, Yuanqing H, Wenlin A, Wei Z, Weihong C, Tengfei Y, Yamin W and Theakstone W H 2012

- The decreasing wind speed in southwestern China during 1969–2009, and possible causes *Quat. Int.* **263** 71–84
- Yang H, Chen J and Pang X 2018 Wind turbine optimization for minimum cost of energy in low wind speed areas considering blade length and hub height *Appl. Sci.* **8** 1202
- Zeng Z *et al* 2019 A reversal in global terrestrial stilling and its implications for wind energy production *Nat. Clim. Change* **9** 979–85
- Zha J, Wu J, Zhao D and Yang Q 2017 Changes of the probabilities in different ranges of near-surface wind speed in China during the period for 1970–2011 *J. Wind Eng. Ind. Aerodyn.* **169** 156–67
- Zhou L, Zeng Z, Azorin-Molina C, Liu Y, Wu J, Wang D, Li D, Ziegler A D and Dong L 2021 A continuous decline of global seasonal wind speed range over land since 1980 *J. Clim.* **34** 9443–61